

# A CALIBRATION PROCEDURE FOR ON-WAFER DIFFERENTIAL LOAD-PULL MEASUREMENTS

## Abstract

*This paper presents a calibration technique for on-wafer differential load-pull measurements. The described calibration procedure makes use of a standard GS/SG calibration substrate only. The calibration accuracy achieved is verified through various independent standards measurement.*

## Introduction

The increased interest in differential and push-pull structures for power amplifier (PA) design has triggered the need of a reliable large signal characterization of differential circuits. A classical single-ended 4-port s-parameter measurement, followed by a transformation to a mixed mode representation<sup>1</sup> is useful in the small signal analysis of 4-port circuits, but proves to be inadequate for large signal characterization. In<sup>2</sup> a differential load-pull system was introduced using hybrid junctions to provide the differential signal to the DUT. In this work, we explain the procedure used for the differential on-wafer calibration of the VNA in full detail. The procedure presented, avoids the use of a differential calibration kit substrate, which is, to the knowledge of the author, not commercially available<sup>3</sup>. For this reason we will use conventional GS/SG standards for our calibration, providing a fully differential characterization of the DUT for load-pull measurements, including the differential input reflection coefficient ( $\Gamma_{diff}$ ) and the power gain ( $G_p$ ). Various verification measurements are presented to illustrate the calibration accuracy; in conclusion the consistency between a differential load-pull measurement and 4-port small signal s-parameter data is investigated at a relative low power level. The paper is divided into three parts: first, we give the procedure to correctly characterize the dual-line probe, secondly, the characterization of the hybrid

and the reformulation of the complete input network (hybrid and probes) as a two-port matrix is developed. In conclusion, the verification of the complete procedure through the measurements of independent standards is shown.

## Dual-Line Probe Data

The dual-line probes used in this work are Cascade GSSG, 200  $\mu\text{m}$  pitch. In order to correctly shift the reference plane to the probe tips a 4 x 4 matrix of the dual-line probe is required. This information is obtained through a two step procedure.

First, we perform a one port Short-Open-Load (SOL) calibration at reference plane 1 (Figure 1). Secondly, the cable is connected to port 1 of the probe while port two of the probe is terminated with 50 ohm and another SOL calibration is performed but now at the probe tip (reference plane 2).

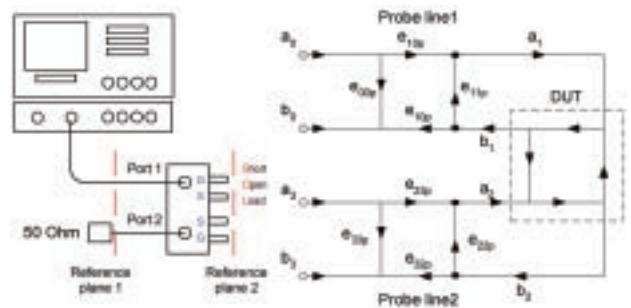


**Figure 1: Dual-Line Probe Cal Procedure (left), 8-Terms Error Box of the Dual-Line Probe (right).**

By downloading the 3 error terms of the two calibrations from the VNA it is possible to extract the network of the probe line ( $e_{00p}, e_{10p}e_{01p}$  and  $e_{11p}$ ). Note that the term  $e_{10p}e_{01p}$  represents the  $S_{12}S_{21}$  of a single probe line, which can be considered as a passive reciprocal network. Consequently, the magnitude of  $S_{12}$  and  $S_{21}$  is determined by the square root of  $e_{10p}e_{01p}$  and the sign of the root can be obtained by imposing the continuity of the phase of  $S_{21}$



versus frequency. **Figure 1** shows the 8 error term model for the dual-line probe. To illustrate the accuracy of this method, **Figure 2** gives the comparison of the 3 standards at reference plane 2, using the direct calibration at the probe tips and using the calibration at reference plane 1, followed by the deembedding of the GSSG probe line. Note that the representation of the dual-line probe by the 8 error term model is only valid when the cross talk between the lines can be neglected. To account for this, **Figure 3** shows the high isolation between port 1 and 2 using an open and two single-ended short conditions (higher than 35 dB up to 3 GHz). Consequently, the dual-line probe can be considered as a 4 x 4 matrix in which the cross terms between the two lines are set to zero.

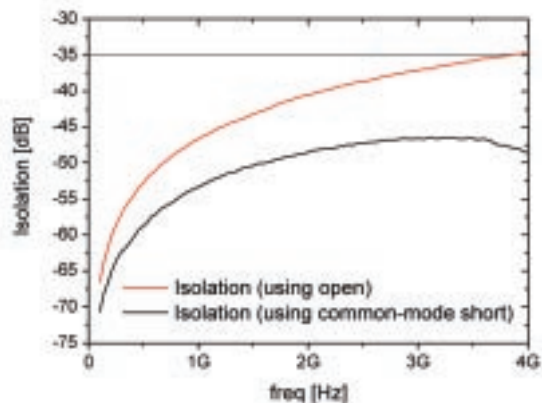


**Figure 3: Dual-Line Probe Isolation.**

### Embedding the Hybrid Junction

The hybrid used in the measurement setup is a Macom H-184 hybrid junction for the 30 MHz — 3 GHz band. The hybrid was characterized using a full four-port s-parameter measurement with the ATN-4000 4-port test set<sup>4</sup>. The cable, bias tees and adapters were included in the measurement of the hybrid. After the hybrid characterization, the two 4 x 4 matrixes (hybrid and dual-line probe) can be combined (**Figure 4**) in order to obtain the matrix representing the complete network from the output of the tuner up to the wafer reference plane. Under realistic load-pull measurement conditions, the stimulus of interest is the differential signal, therefore the common mode port ( $\Sigma$ ) of the hybrid (**Figure 4**) can be terminated with 50 ohm, allowing a matrix reduction to a 3-port. Then using the mixed mode representation, we can describe the above-defined 3-port network as having a single ended input and two mixed-mode output ports (**Equation 1**) to be connected to the differential DUT. In this way, the common mode term  $S_{cc}$  and the mode-conversion terms  $S_{pc}$  and  $S_{cp}$  are clearly identified in the 3 x 3 matrix representing the network.

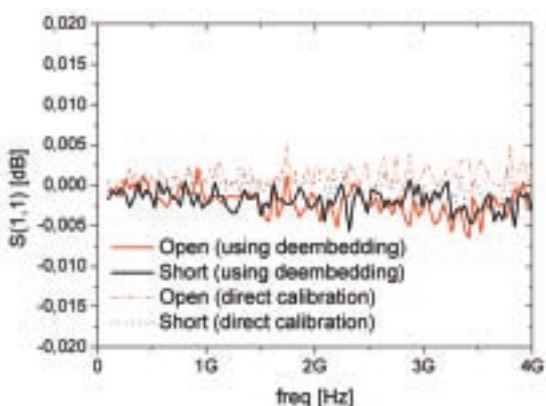
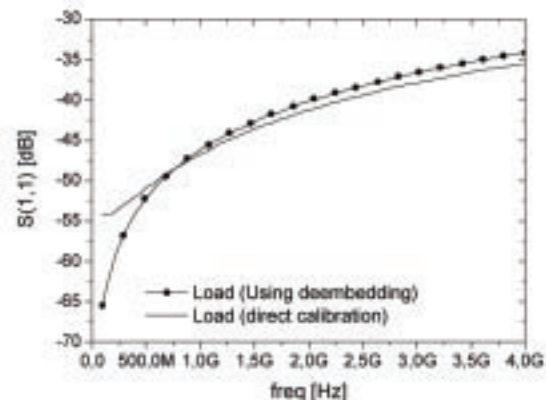


**Figure 2: Comparison of SOL Standard of a Single Line of the Probe Between Cal. at Ref.2 and Cal at Ref. 1 Plus Deembedding.**

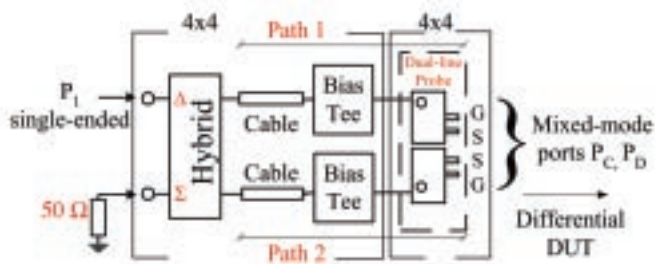


**Figure 4: Hybrid and Dual-Line Probe Embedding.**  
 $P_1$  Single-Ended Port,  $P_c$   $P_d$  Mixed Mode Ports.



$$\begin{bmatrix} b_1 \\ b_c \\ b_d \end{bmatrix} = \begin{bmatrix} S_{11} & \frac{1}{\sqrt{2}}(S_{12} + S_{13}) & \frac{1}{\sqrt{2}}(S_{12} - S_{13}) \\ \frac{1}{\sqrt{2}}(S_{31} + S_{21}) & \frac{1}{2}(S_{22} + S_{23} + S_{32} + S_{33}) & \frac{1}{2}(S_{22} - S_{23} + S_{32} - S_{33}) \\ \frac{1}{\sqrt{2}}(S_{21} - S_{31}) & \frac{1}{2}(S_{22} - S_{23} - S_{32} - S_{33}) & \frac{1}{2}(S_{22} - S_{23} - S_{32} + S_{33}) \end{bmatrix} \begin{bmatrix} a_1 \\ a_c \\ a_d \end{bmatrix} = \begin{bmatrix} S_{SS} & S_{SC} & S_{SD} \\ S_{CS} & S_{CC} & S_{CD} \\ S_{DS} & S_{DC} & S_{DD} \end{bmatrix} \begin{bmatrix} a_1 \\ a_c \\ a_d \end{bmatrix} \quad (1)$$

Equation 1.

$$\begin{bmatrix} b_1 \\ b_d \end{bmatrix} = \begin{bmatrix} S_{11} & \frac{1}{\sqrt{2}}(S_{12} - S_{13}) \\ \frac{1}{\sqrt{2}}(S_{21} - S_{31}) & \frac{1}{2}(S_{22} - S_{23} - S_{32} + S_{33}) \end{bmatrix} \begin{bmatrix} a_1 \\ a_d \end{bmatrix} = \begin{bmatrix} S_{SS} & S_{SD} \\ S_{DS} & S_{DD} \end{bmatrix} \begin{bmatrix} a_1 \\ a_d \end{bmatrix} \quad (2)$$

Equation 2.

Since the mode conversion of the dual-line probe (Figure 3) and the one of hybrid junction (Figure 5) are at least 30 dB down for the frequency of interest (up to 3 GHz), we can neglect the common mode wave terms of (Equation 1) yielding a 2 x 2 matrix (Equation 2). This 2 x 2 matrix can be used to perform the direct single ended to on-wafer differential deembedding.

Consequently, this matrix is used to calculate the 3 error terms of the input network. Please note that this error box includes the different line lengths of path 1 and 2 (see Figure 4 and definition of  $S_{ps}$  and  $S_{sp}$  in Equations 1 and 2) up to the probe and all non-idealities of the hybrid. When uploading this error network in the VNA, the instrument shows directly the  $\Gamma_{diff}$ . All the data presented in the next section was obtained using the network analyzer, calibrated with the previously described procedure.

### Verification of the Calibration

A differential open, two single ended shorts (representing a common and differential mode short simultaneously) and a differential short/common mode open (Figure 6) were used to verify the accuracy of the calibration procedure. Figures 7 and 8 show the magnitude of the reflection coefficient of the measured standards while the phase relation can be examined on the magnified Smithcharts (Figure 8).

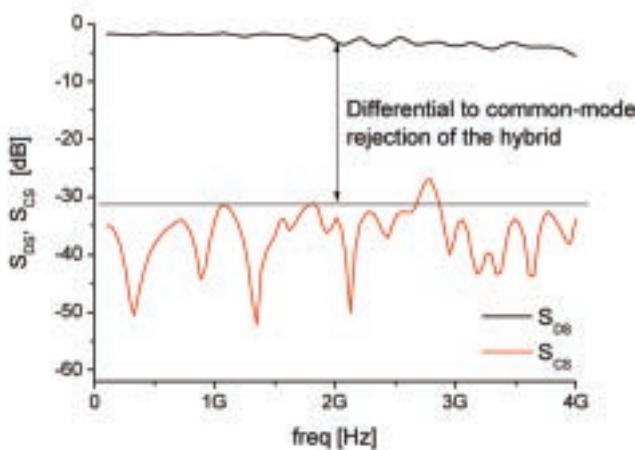
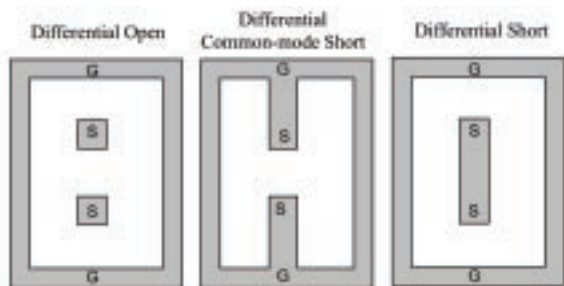
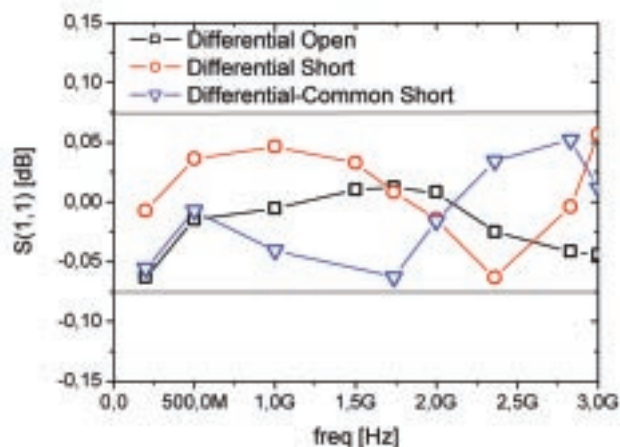


Figure 5: Hybrid Differential to Common-Mode Rejection.



**Figure 6:** Differential Standards for Verification of the Calibration.



**Figure 7:** Differential Calibration Accuracy: Magnitude of Reflection Coefficient of Differential Standards (Figure 5).

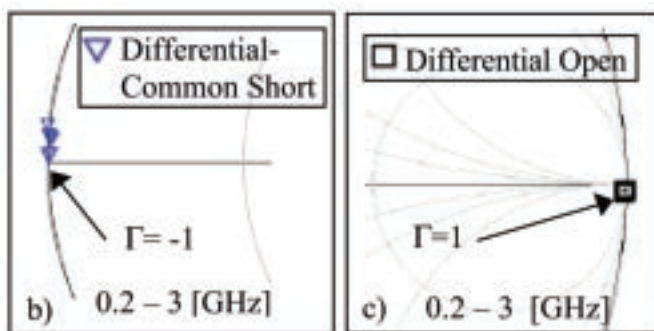


**Figure 8:** Differential Calibration Accuracy:

- a) Magnified Smithchart Inductive Behavior of Differential-Common Short,
- b) Magnified Smithchart Capacitive Behavior of Differential Open.

To illustrate that the procedure corrects the non-idealities of the hybrid block (Figure 4 and definition of  $S_{ps}$  and  $S_{sp}$  in Equations 1 and 2) the measurement of a differential open for two sets of hybrid cables and bias tees, which we will denote briefly as hybrid 1 and hybrid 2, are performed.

Figure 9 shows the measured differential open for the two configurations (hybrid 1 and 2). The perfect agreement validates the above considerations.

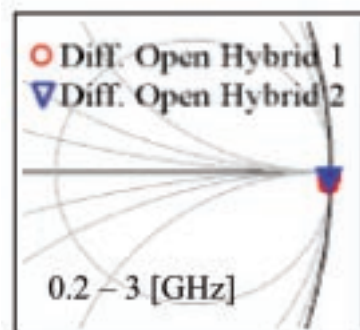


**Figure 9:** Differential Open Measurement Using Configuration with Hybrid 1 and Hybrid 2.

### Differential Load-Pull

The differential load-pull set up shown in Figure 7 utilizes the described deembedding procedure. In Figure 8, the  $G_p$  load contour of a linear 2 GHz InGaP HBT driver amplifier<sup>5</sup> is compared to the power gain circles calculated from a 4-port small signal s-parameter measurement. Since the power levels are small in both measurement conditions, we find an excellent agreement between the differentially driven configuration and the single port excitation used in the full 4-port characterization. This illustrates the high accuracy of the calibration procedure used in the complete load-pull setup. When driven closer into compression these results will start to differ and only the data obtained from the differentially driven amplifier (load-pull analysis) will be meaningful.

### Conclusion

A new, simple, reliable calibration procedure for the on-wafer measurement of differential circuits has been



presented. Theory and measured results are found to be in excellent agreement.

## Acknowledgment

The authors would like to thank DIMES staff for the building of the differential standards and Dr. Mahmoudi for initial work on the differential load-pull system.

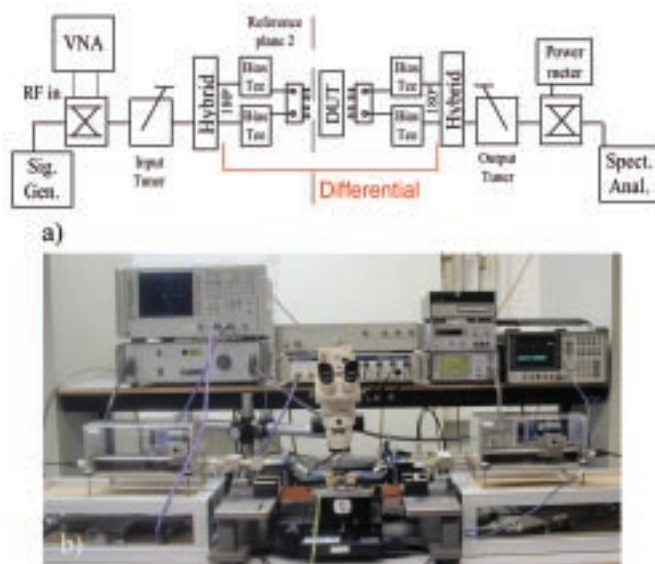


**Figure 10:** Differential Load-Pull:

- a) Block scheme.
- b) Picture of measurement setup.

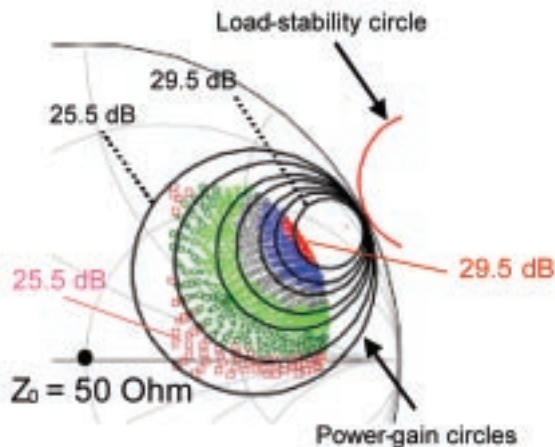


**Figure 11:** Load-Pull Gain Contour Circles for the InGaP HBT Driver Amplifier vs.  $G_p$  Circles Extracted from 4-port S-parameter Measurement.

## References

- 1 Bockelman, D. E. and Eisenstadt, W. R. "Pure-mode Network Analyzer for On-Wafer Measurements of Mixed-Mode S-Parameters of Differential Circuits". *Microwave Theory and Techniques*, IEEE Transactions on Vol. 45, Number 7, pp. 1071-1077, July 1997.
- 2 Mahmoudi, R., Spirito, M., Valk, P., and Tauritz, J. L., "A Novel Load and Source Tuning System for Balanced and Unbalanced WCDMA Power Amplifiers". *Digest of 54th ARFTG*, December 1999.
- 3 Bockelman, D. E. and Eisenstadt, W. R. "Pure-mode Network Analyzer for On-Wafer Measurements of Mixed-Mode S-Parameters of Differential Circuits". *Microwave Theory and Techniques*, IEEE Transactions on Vol. 45, Number 7, pp. 1071-1077, July 1997.
- 4 Schindler, M., Phillips, P., Fennelly, M., Adamian, V., and Enquist, P., "Characteristics and Accuracy of a Fully Corrected Four-port Vector Network Analyzer". *Digest of 50th ARFTG*, December 1997.
- 5 Van der Heijden, M. P., Spirito, M., de Vreede, L. C. N., Van Straten, F., and Burghartz, J. N. "A 2 GHz High-Gain Differential InGaP HBT Driver Amplifier Matched for High IP3" to be published in *2003 IEEE MTT-S Digest*, June 2003.

M. Spirito  
 M. P. van der Heijden  
 M. de Kok  
 L. C. N. de Vreede  
**Laboratory of Electronic Components,  
 Technology & Materials, DIMES,  
 Delft University of Technology  
 The Netherlands**

Reprinted From  
 61st ARFTG Conference Digest  
 Measurement Accuracy  
 Philadelphia, Pennsylvania  
 June 13, 2003